

# The Dark Ages of the Universe and Hydrogen Reionization

Aravind NATARAJAN<sup>1\*)</sup> and Naoki YOSHIDA<sup>2,3</sup>

<sup>1</sup>*Department of Physics and Astronomy & Pittsburgh Particle physics, Astrophysics and Cosmology Center, University of Pittsburgh, 100 Allen Hall, 3941 O'Hara Street, Pittsburgh, PA 15260, U.S.A.*

<sup>2</sup>*Department of Physics, University of Tokyo, Bunkyo, Tokyo 113-0033, Japan*

<sup>3</sup>*Kavli Institute for the Physics and Mathematics of the Universe (WPI), University of Tokyo, Kashiwa, Chiba 277-8583, Japan*

One of the milestones in the cosmic history is the formation of the first luminous objects and hydrogen reionization. The standard theory of cosmic structure formation predicts that the first generation of stars were born about a few hundred million years after the Big Bang. The dark universe was then lit up once again, and eventually filled with ultra-violet photons emitted from stars, galaxies, and quasars. The exact epoch of the cosmic reionization and the details of the process, even the dominant sources, are not known except the fact that the universe was reionized early on. Signatures of reionization are expected to be imprinted in the cosmic microwave background radiation, especially in its large-scale polarization. Future CMB experiments, together with other probes such as H I 21 cm surveys, will provide rich information on the process of reionization. We review recent studies on reionization. The implications from available observations in a wide range of wavelengths are discussed. Results from state-of-the-art computer simulations are presented. Finally, we discuss prospects for exploring the first few hundred million years of the cosmic history.

## §1. Introduction

The quest for neutral hydrogen in the inter-galactic space has a long history.<sup>1)</sup> Observations in the 1960's surprisingly showed that there is indeed little amount of neutral hydrogen in the inter-galactic medium (IGM). It was then immediately proposed that the IGM itself is in a highly ionized state rather than being neutral. A question then naturally followed: how was the IGM ionized? It was not until 2000 that the so-called Gunn-Peterson trough was finally found in the spectra of distant quasars.<sup>2)</sup> The observations reached an early epoch when cosmic reionization was being completed. Clearly, the inter-galactic gas had been indeed neutral but was ionized at an early epoch by some sources of radiation or by some other physical mechanism.

A number of more recent observations suggest that the universe was reionized early on, in the first several hundred million years. For example, CMB experiments provide information on the epoch of reionization through the measurement of the total Thomson optical depth. The scattering of CMB photons with free electrons is quantified by means of the optical depth:

$$\tau = \int dt c \sigma_T n_e = \int \frac{dz}{H(z)(1+z)} c \sigma_T n_e(z) \quad (1.1)$$

---

\*) E-mail: aravind@pitt.edu

$$\begin{aligned}
&= \frac{c \sigma_T (\rho_{\text{crit}}/h^2)}{100 \text{ km/s/Mpc}} \frac{1}{m_N} \frac{\Omega_b h^2}{\sqrt{\Omega_m h^2}} (1 - Y) \\
&\times \int dz \frac{(1+z)^2}{\sqrt{(1+z)^3 + (\Omega_A/\Omega_m)}} x_e(z) \left[ 1 + \mu(z) \frac{Y}{4(1-Y)} \right].
\end{aligned} \tag{1.2}$$

where  $x_e(z)$  is the ionization fraction,  $c$  is the speed of light,  $\sigma_T$  is the Thomson cross section,  $m_N$  is the nucleon mass, and  $Y$  is the helium fraction. The pristine IGM consists of hydrogen and helium. We set  $\mu(z) = 0$  if helium is neutral, 1 if singly ionized, and 2 if doubly ionized. The large-scale polarization of the cosmic microwave background measured by the WMAP satellite suggests that reionization – release of free electrons – began as early as  $z \sim 10$ .<sup>3)</sup> There are also other indirect probes, from the cosmic infrared background to the distribution of star-forming galaxies at  $z > 6$ . The ionized fraction, or alternatively the neutral fraction, of the IGM can be measured in multiple ways.<sup>4)</sup> Ultimately, all such observations must be explained as outcomes of a series of events that affected the ionization and thermal state of the IGM in the early cosmic history.

Theoretical studies on reionization naturally include the formation of the first cosmic structures.<sup>7)</sup> In this article, we first review recent progress in the theory of structure formation in the early universe. We then give an overview of probes of cosmic reionization and the Dark Ages. We put our emphasis on the use of hydrogen 21 cm emission and absorption to be observed in the currently operating and future radio telescope arrays. We conclude the present article by discussing the prospects for direct and indirect observations of reionization.

## §2. Early structure formation

We begin by describing structure formation in the standard cosmological model. The primordial density fluctuations predicted by popular inflationary universe models have very simple characteristics; the fluctuations are nearly scale invariant and the corresponding mass variance is progressively larger at smaller masses.<sup>6)</sup> Theoretical studies and numerical simulations of early structure formation based on such models suggest that the first cosmic structures form as early as when the universe is one hundred million years old.<sup>8),9)</sup>

Dense, cold clouds of self-gravitating molecular gas develop in the inner regions of small dark matter halos and contract into proto-stellar objects with masses of about several hundreds of solar-masses. Figure 1 shows the projected gas distribution in a cosmological simulation that includes hydrodynamics and primordial gas chemistry.<sup>10)</sup> Star-forming gas clouds are found at the knots of filaments, which resemble the large-scale structure of the universe, although actually much smaller in mass and size.

As soon as the first stars are formed, they emit light and flood the universe with ultra-violet photons. While some of the gas clouds actually bear stars, other clumps, the so-called minihalos, remain as neutral gas clouds which might be significant sinks of photons via recombination processes later during the epoch of reionization.<sup>39)</sup> It

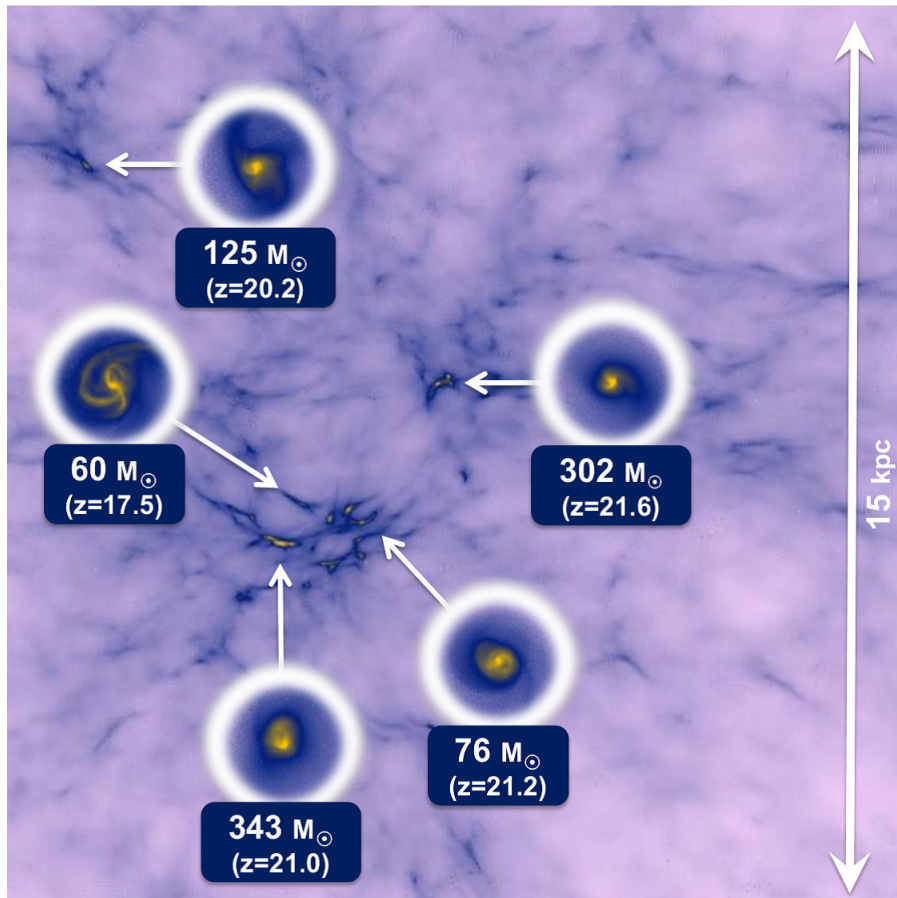


Fig. 1. The matter distribution in the early universe. The plotted region is a cube of 15 kpc on a side. First stellar nurseries are found at the knots of the filamentary structure. The insets show the fine structure of the star-forming regions. Also the final masses of the newly born stars are indicated. From Ref. 10).

is generally thought that cosmic reionization is likely initiated by the first generation of stars but that the major role is taken over by larger and more luminous objects. Thus the emergence of the first galaxies is a critical event in the early cosmic history.

The observational frontier extends beyond  $z = 6$ , reaching recently to  $z = 10$ . Utilizing the unprecedented near-IR sensitivity of the Wide Field Camera 3 on board the *Hubble Space Telescope*, deep images of the Hubble Ultra Deep Field and other fields opened up a fantastic view into the high-redshift Universe. The galaxy luminosity function at  $z > 6$  has been derived from the combined observations by HST and by large ground-based telescopes.<sup>25), 26)</sup> Interestingly, the observed high-redshift galaxies *cannot* be the major source of reionization.<sup>27)</sup> This can be easily seen by integrating the luminosity function down to the faint limit detected.<sup>28)</sup> It is thus suggested that very faint (proto-)galaxies are needed to ionize the IGM perhaps at  $z \sim 10$ . Other faint sources such as small quasars may also be worth being

considered, as we discuss in Section 4.

In the standard  $\Lambda$  Cold Dark Matter model, where structure grows hierarchically, the first stars are formed before bigger and more luminous galaxies emerge. Feedback effects from the stars are thus expected to play a vital role in setting the scene, *i.e.*, the *initial conditions*, for first galaxy formation.<sup>22)</sup>

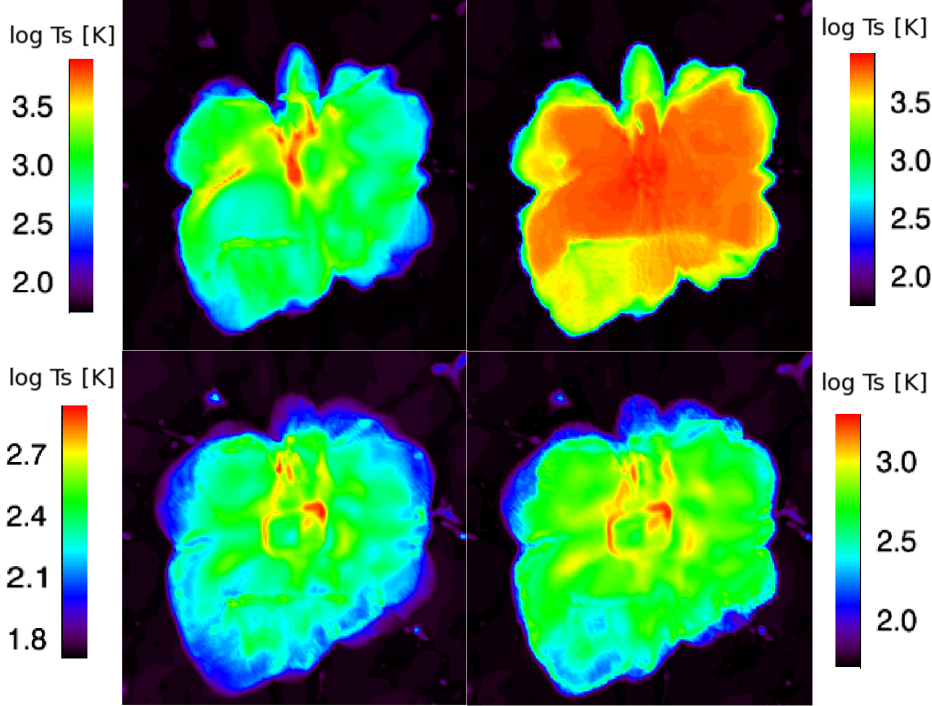


Fig. 2. The first HII region around a massive Population III star. The plotted region is a cube of 3 kilo-parsecs on a side. The color scale shows the spin temperature of 21 cm emission. From Ref. 11).

### §3. The first light and HII regions

The birth of the first generation of stars has important implications for the thermal state and chemical properties of the IGM in the early universe. As soon as the first stars are formed, they emit a copious amount of UV photons and then generate HII regions. The formation of early HII regions were studied by a few groups using radiation hydrodynamics simulations.<sup>49),50)</sup> It is expected that there are numerous early relic HII regions formed by the first stars at  $z = 15 - 30$ . Although individual HII regions are too small and too faint to be observed in any wavelength, they may collectively imprint distinguishable fluctuations in the rest-frame 21 cm. Figure 2 shows the brightness temperature of an early relic HII region in a cosmological simulation.<sup>11)</sup> The relic HII region has a large 21 cm spin temperature and thus is bright in radio, yielding a brightness temperature of  $\sim 1$  mK. However, its physical size of a few kilo-parsecs hampers direct observations for it to be an individual point source.

Nevertheless, clustering of such HII regions will leave detectable imprints in 21 cm emission.<sup>14)</sup>

Large-scale HII regions around galaxies and perhaps early galaxy groups, extending over tens of mega-parsecs, are probably dominant in volume at lower redshift of  $6 < z < 10$  where the ongoing observation by LOFAR is aimed at.<sup>13)</sup> Numerical simulations show complex topological features of ionized and neutral regions in a large cosmological volume. Ultimately, the overall morphology of the HII bubbles will provide invaluable information on the sources of reionization and on how the process occurred in the first one billion years.<sup>17)</sup>

Early HII regions generate secondary CMB anisotropies via the kinetic Sunyaev-Zeldovich effect.<sup>12)</sup> Figure 3 shows the large-scale ionization structure and the generated CMB fluctuations calculated from state-of-the-art  $\Lambda$ CDM simulations with radiative transfer. Note that the simulation covers a volume of more than 100 co-moving Mpc on a side. Large HII bubbles are generated not by a single luminous galaxy but by a group of at least tens of star-forming galaxies. Highly inhomogeneous distribution of the HII regions boosts the fluctuations of the CMB at small angular scales. The amplitude and the shape of the angular power-spectrum can be used to infer the duration of reionization and the overall inhomogeneity of ionized regions as can be seen in Figure 3.

Recent observations by the South Pole Telescope (SPT) collaboration<sup>115)</sup> have placed an upper limit on the CMB temperature fluctuations from the kinematic SZ effect at  $l = 3000$  to be  $D_{\text{patchy},3000} < 4.9 \mu\text{K}^2$  at the 95% confidence level when the degree of angular correlation between the thermal Sunyaev-Zeldovich and the cosmic infrared background is allowed to vary. The SPT result suggests that reionization ended at  $z > 5.8$  at 95% confidence (accounting for the tSZ-CIB correlation), in good agreement with other observations. We will discuss the current constraints and the prospects for observations of CMB temperature fluctuations in more substantial detail later in Section 7.

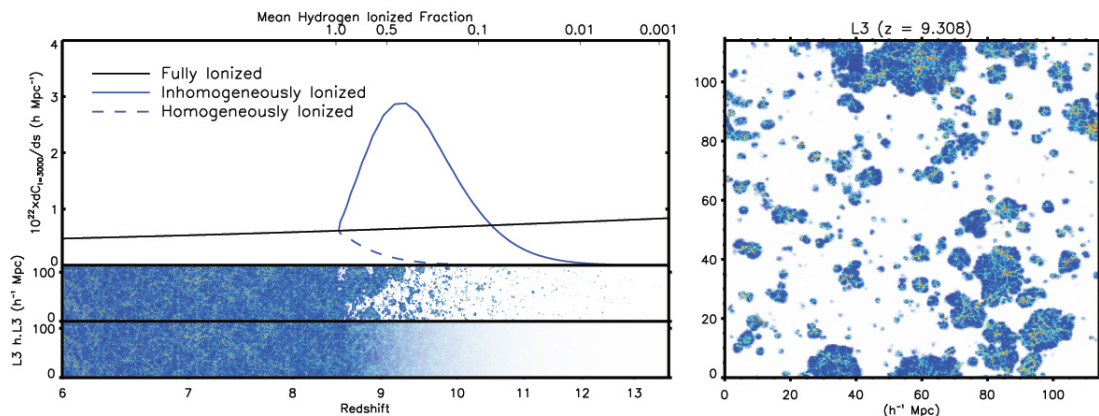


Fig. 3. Simulations of the kinematic SZ effect caused by early HII regions. The left panel shows the contribution to the angular power spectrum from a given redshift. The right panel shows a snapshot at  $z = 9.3$  for a volume of 120 Mpc on a side. From Ref. 12).

#### §4. Imprints of dark matter

There could be sources of reionization other than stars and galaxies, including somewhat exotic possibilities. Partial ionization of the IGM can be caused by X-rays and gamma rays from particle annihilation, and up-scattered CMB photons from inverse Compton scattering.<sup>15),29),30),31),32)</sup> Chen & Miralda-Escudé (2008) argue that X-rays from the first stars heat the surrounding gas and couple the 21 cm spin temperature to its kinetic temperature, generating a large Lyman- $\alpha$  absorption sphere. X-rays from early mini-quasars could also raise the gas kinetic temperature and enhance 21 cm signals.<sup>16)</sup> Regardless of the nature of the sources, reionization by X-rays lead to more diffuse distribution of ionized gases. The particle nature of dark matter may have observable effects on the mass and luminosity of the earliest stars.<sup>33),34),35),36)</sup>

High-energy particles and photons that are produced by decay or annihilation of dark matter (DM) can also ionize the IGM partially. It is unlikely that significant energy release from DM occurred early on, because even a small deviation from the well-established thermal and ionization history of the universe already places rather tight constraints.<sup>37),38)</sup> However, if energy release occurred late, characteristic signals may be imprinted in the CMB and in the 21 cm signal. Recent studies suggest that future radio telescopes can indeed detect signals from DM annihilation.<sup>18),19)</sup> We will devote more detailed discussion later in Section 7.

The nature of particle dark matter can affect the early evolution of the IGM in an indirect but interesting way. A combined analysis of high-redshift galaxy number counts, other star formation indicators such as supernovae rate, and the epoch of reionization can be used to infer the overall growth of sub-galactic structure in the Dark Ages.<sup>20)</sup>

It is known that models with warm dark matter, in which dark matter particles possess substantial thermal motions, predict less abundant small-scale structures. The fact that the universe was reionized early on strongly suggests that structure formation and the associated star formation must have occurred similarly early. Accurate measurement of the Thomson optical depth of the CMB and also of the visibility function (the derivative of the optical depth with respect to redshift) can give constraints on the nature of dark matter, if the derived optical depth is sufficiently large.<sup>21)</sup>

#### §5. Infrared background

The extragalactic infrared background (IRB) is largely contributed by accumulated light emitted from galaxies and quasars. The local source, most significantly the Zodiacal light, and the stellar emission from low-redshift galaxies are the two dominant sources, but the remaining IR flux may be either from high-redshift galaxies or from low surface brightness galaxies in the local universe. An interesting possibility is that, if Pop III stars were formed at  $z = 10 - 20$ , UV photons emitted from them, redshifted to 1-5  $\mu\text{m}$  in the present-day universe, are expected to contribute to the IRB. In principle, the IRB can be used to constrain the star formation

activity in the early universe, which should be consistent with what other probes of cosmic reionization suggest. Interestingly, a recent cross-correlation analysis of IRB and X-ray indicate that AGNs or some IR sources associated with them contributes appreciably to about 10 percent of the IRB.<sup>48)</sup>

It has been long speculated from an apparent bump in the IRB at 1-2 micron<sup>40)</sup> that a significant amount of hot Population III stars were formed at  $z \sim 10$  (see Figure 4). The bump, if real, can be explained largely by photons near Lyman- $\alpha$  wavelength redshifted from  $z = 10$  to  $z = 0$ . Such an intense formation of massive Population III stars at  $z \sim 10$ , when substantial metal enrichment must have already occurred, is not expected in popular models of first star formation. However, it remains still controversial whether or not an early generation of stars and galaxies contribute to the IRB.<sup>44)</sup> The overall amplitude of the IRB, estimated from the spectra of distant TeV blazars for example, still allows small contribution from unknown sources,<sup>41)</sup> and the IRB fluctuations measured by Spitzer and Akari both suggest that the fluctuation power spectra can be explained by clustered sources at high redshifts.<sup>42),43)</sup> The low-level shot noise features and the shape of the power spectra at sub-degree scales may be reconciled by intra-halo stars around galaxies at  $z = 1 - 4$ .<sup>47)</sup> A concerted use of multi-wavelengths observations will be needed to distinguish various models and pin down the sources of reionization.

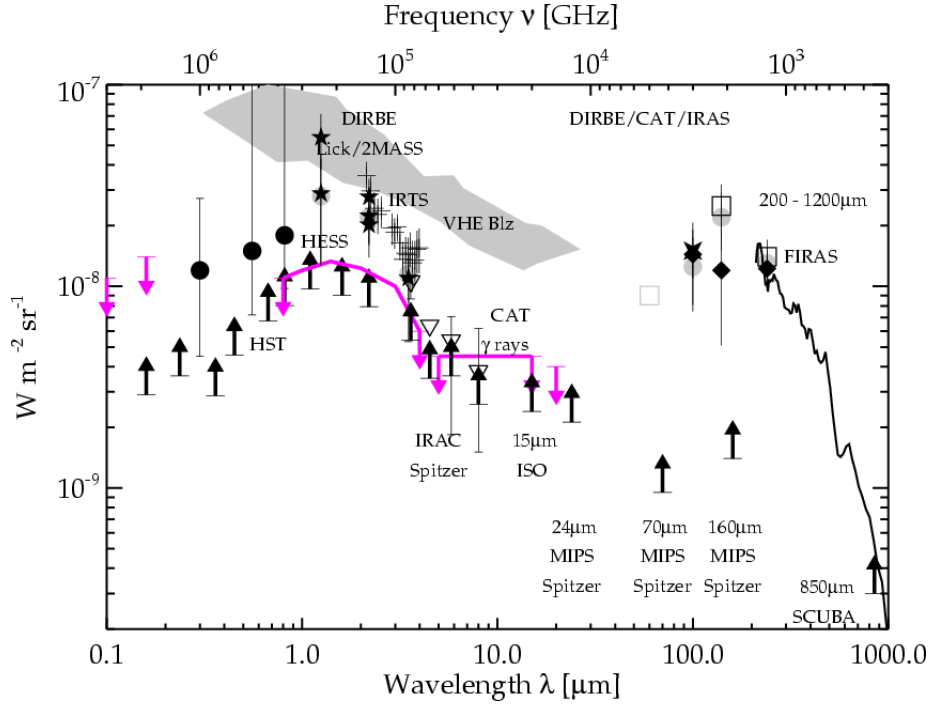


Fig. 4. The observed spectrum of the cosmic infrared background. From Ref. 45).

## §6. Probes of reionization

From observations of the spectra of distant quasars, it is known that the Universe is highly ionized today.<sup>2), 55), 56), 57)</sup> Evidence for reionization at the  $5.5\sigma$  level was obtained by the Wilkinson Microwave Anisotropy Probe (WMAP) measurement of the CMB EE polarization power spectrum.<sup>58)</sup>

Reionization began at a redshift  $z \sim 20 - 30$  when the first stars were formed. Later, Population II stars, star forming galaxies, and active galactic nuclei completed the process.<sup>59), 60), 61), 62), 63), 64)</sup> The precise details of the reionization process are not known, and must be inferred from observations. Let us now discuss two promising probes of reionization - the 21 cm spin flip of neutral hydrogen, and the cosmic microwave background.

### 6.1. Probing the dark ages through 21 cm observations

The nature of the earliest stars is a fascinating topic, but one which is very difficult to study due to the lack of observations. Emission and absorption due to the 21 cm spin flip transition of neutral hydrogen have emerged as useful techniques to probe the epoch of primordial star formation.<sup>77), 65), 66), 67), 68), 70), 70), 71), 72), 73)</sup> Before the formation of the first luminous objects, the spin temperature of neutral hydrogen is typically close to the CMB temperature at a redshift  $z \sim 20$  because the gas is not dense enough to collisionally couple the spin temperature to its kinetic temperature.<sup>65)</sup> The formation of the first stars however, results in the production of Lyman- $\alpha$  photons which can couple the spin and kinetic temperatures of neutral hydrogen through the Wouthuysen-Field mechanism.<sup>74), 75)</sup> The kinetic temperature of the gas  $T_k \propto (1+z)^2$  is typically lower than the CMB temperature  $T_\gamma$  (which scales as  $(1+z)$ ) at  $z \sim 20$ .

The Wouthuysen-Field mechanism sets  $T_s = T_k$ , so the turn-on of the first stars produces a significant decrease in the 21 cm brightness temperature ( $T_b$ ) around the redshift of first star formation, with  $T_b \propto (T_s - T_\gamma)/T_s \sim -T_\gamma/T_k$ . We thus expect a significant decrement in the 21 cm brightness temperature  $T_b$  around the redshift of first star formation, since  $T_b \propto (T_s - T_\gamma)/T_s$ . Heating of the gas by ionizing radiation rapidly sets  $T_k > T_\gamma$ , with  $T_b$  entering the saturation regime before decreasing to zero as the Universe reionizes. The magnitude of the decrement in  $T_b$  as well as the width provide valuable information on the properties of the first stars and X-ray sources. The spectral structure allows us to distinguish the signal from the much larger background which is spectrally smooth.

The 21 cm brightness temperature relative to the CMB (also called differential brightness temperature) is given by (see, for example<sup>69)</sup>):

$$T_b \approx 27 \text{ mK } x_{\text{HI}} \sqrt{\frac{1+z}{10}} \left( 1 - \frac{T_\gamma}{T_s} \right), \quad (6.1)$$

where  $x_{\text{HI}}$  is the neutral hydrogen fraction, and  $T_s$  is the spin temperature of neutral hydrogen given by:

$$T_s^{-1} \approx \frac{T_\gamma^{-1} + (x_c + x_\alpha) T_k^{-1}}{1 + x_c + x_\alpha}. \quad (6.2)$$



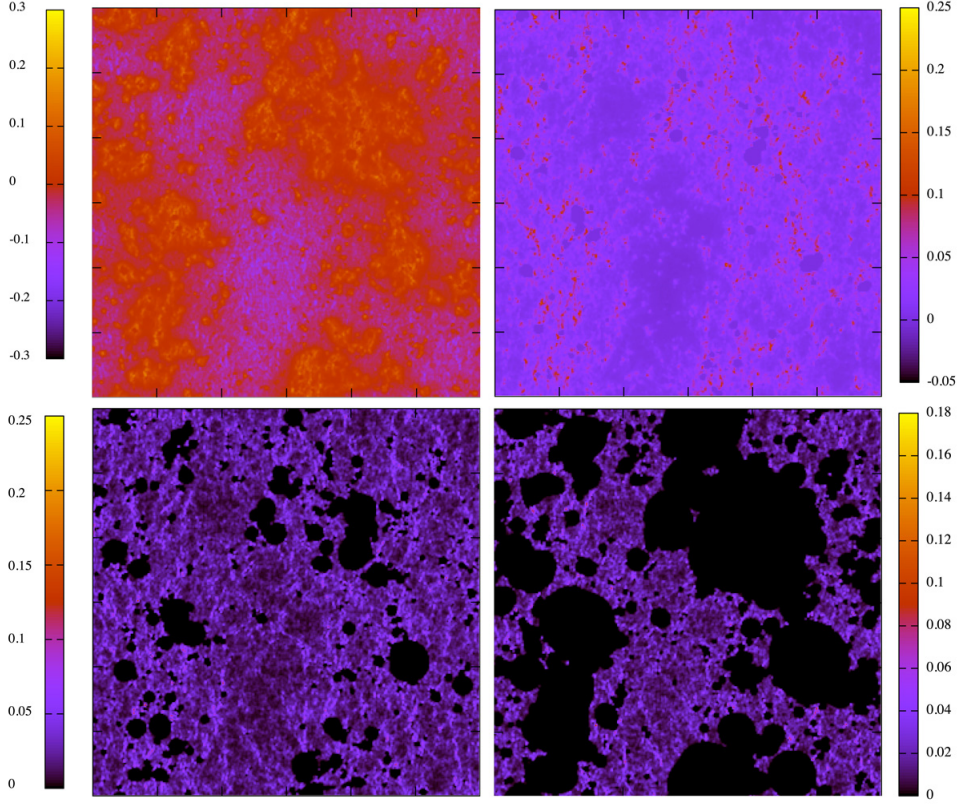


Fig. 5. The large-scale 21 cm fluctuations calculated by SIMFAST. Each panel is  $300 \text{ Mpc} \times 300 \text{ Mpc}$ , and shows the brightness temperature in Kelvin at  $z = 14, 12, 10, 8$  (from top left to bottom right).

$x_c$  is called the collisional coupling coefficient, while  $x_\alpha$  is the Lyman- $\alpha$  coupling due to the Wouthuysen-Field mechanism. Collisional coupling is important when the gas is dense or hot, i.e. at high redshifts. Figure 6(a) shows the collisional coupling and Lyman- $\alpha$  coupling ( $x_\alpha$ ) as functions of redshift (for a particular star formation model). Once star formation begins at a redshift  $z \lesssim 30$ , the Lyman- $\alpha$  coupling provides the dominant contribution. Figure 6(b) shows the gas kinetic temperature for a specific star formation model, as well as the CMB temperature. At very high redshifts ( $z \gtrsim 300$ ), the gas temperature closely follows the CMB temperature due to Compton scattering with residual electrons. At lower redshifts, the gas is not sufficiently dense for Compton scattering to be efficient. The kinetic temperature then falls off  $\propto (1+z)^2$  until star formation begins. Three dimensional maps of the brightness temperature of neutral Hydrogen can be used to infer the reionization history of the Universe. Fig. 5 shows the simulated brightness temperature (for a particular star formation model) in  $300 \text{ Mpc} \times 300 \text{ Mpc}$  boxes at redshifts  $z = 14, 12, 10$ , and  $8$ , obtained using the SIMFAST code.<sup>86)</sup>

The intensity of radiation in the Lyman- $\alpha$  wavelength at any given redshift

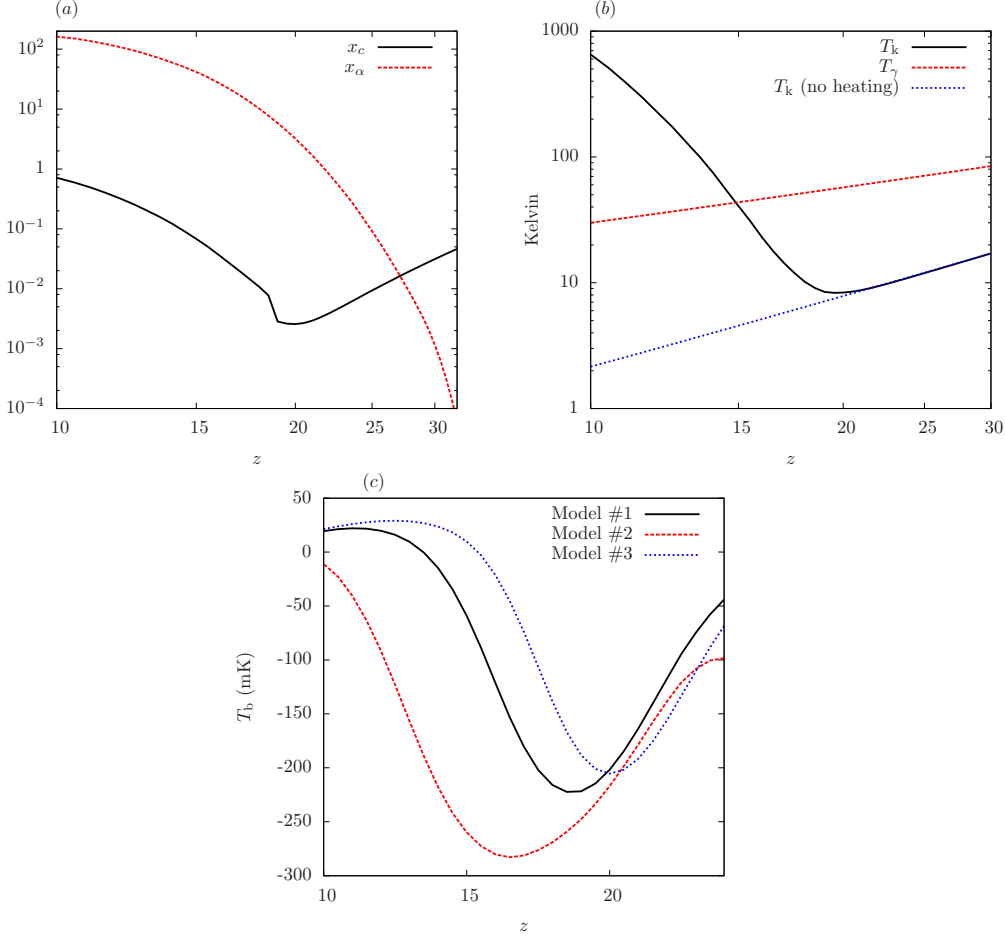


Fig. 6. Panel (a) shows the collisional coupling coefficient compared to the Lyman- $\alpha$  coupling coefficient. At high redshifts, collisional coupling provides the dominant contribution, but after first star formation,  $x_\alpha \gg x_c$ . (b) shows the gas kinetic temperature (solid, black) and the CMB temperature (dashed, red). The dotted (blue) line shows the gas temperature in the absence of heating. (c) shows the 21 cm brightness temperature (relative to the CMB), for three different models that differ in their star formation rate, and X-ray flux.

$z$  is due to radiation emitted between the Lyman- $\alpha$  wavelength and the Lyman limit. Thus radiation emitted at wavelengths shorter than Lyman- $\alpha$ , at a redshift  $z' < z_{\max}(n)$  will redshift until the photons reach the Lyman- $\alpha$  wavelength at a redshift  $z < z'$ . Thus photons with wavelengths between Lyman- $\alpha$  and Lyman- $\beta$  are visible up to a maximum redshift  $z_{\max}(2)$ , where  $1 + z_{\max}(2) = (\lambda_\alpha/\lambda_\beta)(1 + z)$ .<sup>80)</sup> The Lyman- $\alpha$  coupling coefficient  $x_\alpha$  is proportional to the Lyman- $\alpha$  photon intensity:<sup>80)</sup>

$$J_\alpha = \frac{(1 + z)^2}{4\pi} \sum_{n=2}^{n_{\max}} \int_z^{z_{\max}(n)} \frac{cdz'}{H(z')} \epsilon(\nu'_n, z'), \quad (6.3)$$

where  $\epsilon$  is the number of photons emitted per comoving volume, per unit time, per frequency, and depends on the nature of the ionizing sources.

Once the Lyman- $\alpha$  coupling  $x_\alpha \gg 1$ , the spin temperature  $T_s$  is set to the kinetic temperature  $T_k$  of the gas. The redshift at which  $x_\alpha > 1$  is however, sensitive to the nature of the ionizing sources. The initial mass function (IMF) of Pop. III plays an important role in determining the number of Lyman- $\alpha$  and ionizing photons. Authors<sup>81)</sup> find that a  $170 M_\odot$  star emits about 34,500 ionizing photons per baryon over its lifetime, compared to  $\approx 6600$  per baryon per lifetime for a Pop. II star. Authors<sup>82)</sup> find that a heavy IMF with  $M > 300 M_\odot$  produces 16 times as many ionizing photons compared to a Salpeter IMF. Thus, one may hope to place constraints on the nature of Pop. III stars by measuring the brightness temperature of neutral Hydrogen 21 cm radiation, although it will be challenging to break the degeneracy between the primordial star IMF and the star formation rate<sup>86)</sup>

Accretion of gas onto black holes produced by the first stars will generate highly energetic X-rays which heat the gas to temperatures above the CMB. The temperature evolution of the gas in the presence of X-ray heating is given by:

$$-(1+z)H(z)\frac{dT_k}{dz} = -2T(z)H(z) + \frac{2\eta_{\text{heat}}(z)}{3k_b}\xi(z), \quad (6.4)$$

in the limit of ionized fraction  $x_{\text{ion}} \ll 1$ .  $\xi(z)$  is the energy absorbed per atom per unit time at redshift  $z$ .  $\eta_{\text{heat}}$  is the fraction of the absorbed energy that goes into heating. Detailed computations<sup>87),88),89),90)</sup> show that  $\eta_{\text{heat}}$  is a function of photon energy, as well as the ionized fraction. For highly neutral gas  $x_{\text{ion}} \approx 10^{-4}$ , we have  $\eta_{\text{heat}} \lesssim 0.2$  for photon energies  $E_\gamma > 100$  eV. For slightly ionized gas with  $x_{\text{ion}} \sim 0.01$ ,  $\eta_{\text{heat}} \sim 0.4$  for  $E_\gamma > 100$  eV, with lower energy photons contributing more to heating.<sup>87)</sup>

The ratio of temperatures in the absence of any heating is approximately given by  $T_\gamma/T_k \approx 7.66 [20/(1+z)]$ . From Eq. 6.1, it is easy to see that the minimum brightness temperature (relative to the CMB) is  $\approx -300 \sqrt{20/(1+z)}$  mK, when the gas is not heated by X-rays, and when the spin and kinetic temperatures are well coupled by Lyman- $\alpha$  photons. Figure 6(c) shows the brightness temperature of neutral hydrogen relative to the CMB, obtained using the SIMFAST code,<sup>85),86)</sup> for three different models that differ in their star formation efficiency and X-ray heating flux. The location of the trough in  $T_b$ , as well as its width are determined by the physics of primordial star formation, i.e. the Lyman- $\alpha$ , and X-ray flux, which in turn may be related to the star formation efficiency, and X-ray heating rate. It is clear that a precise measurement of the 21 cm temperature will provide important information regarding the formation of the first stars.

## 6.2. Measuring the global 21 cm brightness temperature

Experiments studying the universe through the 21 cm transition include the Precision Array for Probing the Epoch of Reionization (PAPER),<sup>91),92)</sup> the Giant Metrewave Radio Telescope - Epoch of Reionization (GMRT-EoR),<sup>93)</sup> the Low Frequency Array (LOFAR),<sup>94)</sup> the Murchison Widefield Array (MWA),<sup>95)</sup> the Hydrogen Epoch of Reionization Array (HERA),<sup>96)</sup> the Square Kilometer Array (SKA),<sup>97)</sup> the Experiment to Detect the Global EoR Step (EDGES),<sup>98)</sup> the Large Aperture Experiment to detect the Dark Ages (LEDA),<sup>99)</sup> the Sonda Cosmológica de las Islas para la

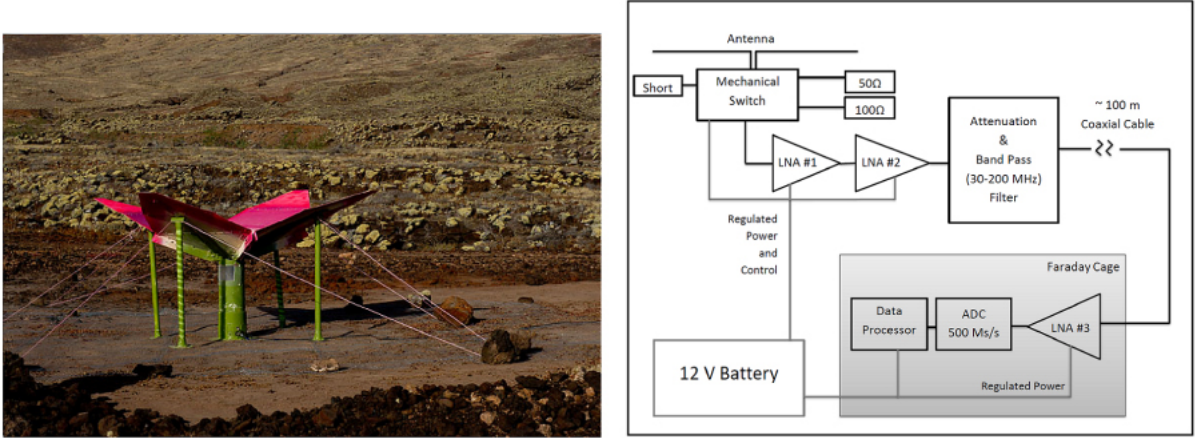


Fig. 7. The SCI-HI experiment showing the antenna on-site at Isla Guadalupe, and the system block diagram. Figure from Ref.100).

Detección de Hidrógeno Neutro (SCI-HI),<sup>100)</sup> and the Dark Ages Radio Explorer.<sup>101)</sup>

*The SCI-HI 21 cm all-sky spectrum experiment:*

The Sonda Cosmológica de las Islas para la Detección de Hidrógeno Neutro (SCI-HI) experiment consists of a single broadband sub-wavelength size antenna and a sampling system for real time data processing and recording.<sup>100)</sup> Preliminary observations were completed in June 2013 at Isla Guadalupe, a Mexican biosphere reserve with minimal infrastructure, located  $\sim 260$  km from the Pacific coast.

Figure 7 shows the antenna on site, as well as a basic block diagram of the instrument. The signal from the antenna passes through a series of electronic stages, including amplifiers and filters to remove radio frequency interference (RFI) below 30 MHz and aliasing of signals above 200 MHz. The system is placed inside a Faraday cage  $\sim 50$  meters from the antenna. The data sampling/processing duty cycle is  $\sim 10\%$ , so 1 day of observation yields about 2 hours of effective integration time.

Calibration of data is performed by comparing the measured brightness temperature to the Global Sky Model of the Galaxy. Figure 8 shows the Global Sky Model of the Galaxy, at 70 MHz, from Ref.<sup>102)</sup> Also shown is the simulated beam pattern of the antenna at Local Sidereal Time (LST) 08:00, 16:00, and 24:00, plotted for the latitude of Guadalupe. The antenna beam is fairly broad  $\sim 55^\circ$  at 70 MHz, and thus, this is low angular resolution experiment. The antenna beam is averaged over the Galaxy. We therefore expect a large sky brightness when the Galaxy is overhead, and a minimum when the Galaxy is aligned with the horizon. This is precisely what we see in the plot to the right. The diurnal variation of the Galactic temperature may be used to subtract the large Galactic foreground, to recover the cosmological 21 cm signal which does not vary with time. The calibrated spectrum is fit to the

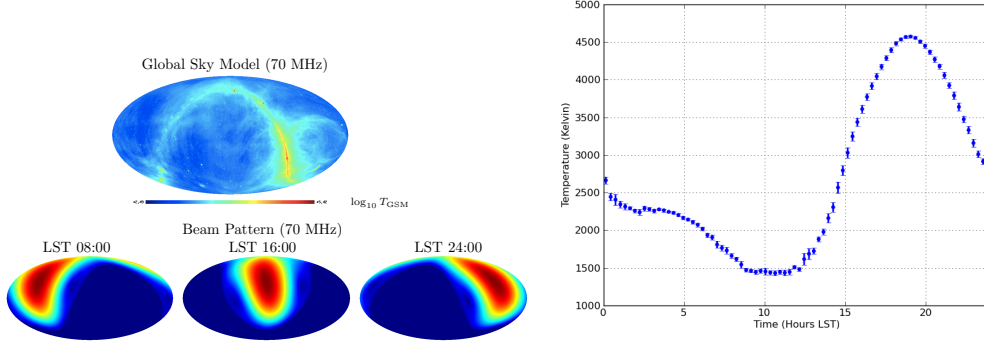


Fig. 8. Sky temperature and antenna beam pattern in (RA,DEC) coordinates. The top row shows the sky temperature (logarithmic units) at 70 MHz, from Ref. 102). Also shown is the simulated antenna beam pattern at 70 MHz at different LST, plotted for the latitude of Isla Guadalupe. Shown on the right is the diurnal variation of a single 2 MHz wide bin centered at 70 MHz, for 9 days of observation, binned in 18 minute intervals. Figure from Ref. 100).

Galactic sky-averaged brightness temperature ( $T_{\text{GM}}$ ):

$$\log_{10} T_{\text{GM}}(\nu) = \sum_{k=0}^n a_k \left[ \log_{10} \left( \frac{\nu}{70 \text{ MHz}} \right) \right]^k \quad (6.5)$$

Using the calculated  $a_k$  for each day of data, the residuals  $\Delta T(\nu) = \langle T_{\text{meas}} \rangle_{\text{DAY}}(\nu) - T_{\text{GM}}(\nu)$  are calculated. These  $\Delta T(\nu)$  values are our estimate of the 21 cm all-sky brightness temperature spectrum after removal of Galactic emission. An  $n = 2$  fit captures the band average expected foreground brightness temperature ( $a_0$ ), a power law spectral shape ( $a_1$ ), and a self-absorption correction term ( $a_2$ ). Adding additional  $a_k$  terms is found to have minimal impact on the overall residual levels.

Residuals obtained after subtraction of the large Galactic foreground are  $\lesssim 20$  Kelvin from 4.4 hours of integration, in the range 60-88 MHz ( $15 < z < 23$ ). Given that the mean foreground is between 2000 - 5000 Kelvin, the residuals obtained by SCI-HI are  $< 1\%$  of the foreground signal. Nevertheless the residuals obtained are nearly two orders of magnitude larger than the cosmological 21 cm brightness temperature. Improvements in system design are currently underway. Data collection is expected to resume in the Summer of 2014, at Isla Socorro, or Isla Clari3n which are exceptionally radio quiet sites.

#### *The Dark Ages Radio Explorer:*

Even the most remote regions on Earth suffer from some man-made radio frequency interference, as well as ionospheric effects. The Dark Ages Radio Explorer (DARE)<sup>101)</sup> is a space based cosmology mission that aims to detect the redshifted 21 cm brightness temperature in the frequency range 40-120 MHz ( $11 < z < 34$ ). DARE will orbit the moon for a mission lifetime of 3 years, and will collect data above the lunar farside, free from radio frequency interference, ionospheric effects, and heliospheric emissions. Thus, DARE is expected to shine light on primordial

star formation: in particular DARE expects to place useful bounds on the epoch of first star formation, the formation of the first accreting black holes, and the start of the reionization epoch.

The DARE radiometer consists of a dual-polarized antenna with a compact, integrated, front-end electronics package, a single-band, dual-channel receiver, and a digital spectrometer. The antenna consists of a pair of bi-conical dipoles, made unidirectional by a set of deployable radials attached to the spacecraft bus that act as an effective ground plane. The receiver provides amplification of the antenna signal to a level sufficient for further processing by the digital spectrometer, and incorporates a load switching scheme to assist calibration. There are two receivers to accommodate the antennas, i.e. one receiver per antenna polarization. Noise diodes provide a reliable additive noise temperature during operation. The noise diodes will be used to monitor spectral response and linearity of downstream components. The instrument design is coupled to a multi-tiered calibration strategy to obtain the RF spectra from which the 21 cm signal can be extracted. The calibration strategy relies on the fact that a high degree of absolute calibration is not required, but focuses on the relative variations between spectral channels, which are much easier to control.

The antenna power pattern covers approximately 1/8 of the sky depending on frequency, and the data set will consist of spectra from 8 independent regions on the sky. DARE uses four free parameters to fit the foreground, i.e.  $\log T_{\text{FG}} = \log T_0 + a_1 \log \nu + a_2 (\log \nu)^2 + a_3 (\log \nu)^3$ . The parameter values are fit separately, to each sky region. Thus, there are 32 foreground parameters in total. It is possible to separate the signal from the large foregrounds because the foregrounds are spectrally smooth, while the 21 cm brightness temperature has spectral structure. Also the foregrounds are spatially varying, while the 21 cm temperature is spatially smooth. With three years of observation, the DARE mission is expected to obtain 3000 hours of integration. The experiment is expected to constrain the epoch of first star formation to  $\sim 9\%$  accuracy, the start of X-ray heating by accreting black holes to  $\sim 1.4\%$  accuracy, and the start of reionization to  $\sim 0.4\%$  accuracy.

Both SCI-HI and DARE expect to measure the *global* 21 cm signal. The *power spectrum* of 21 cm fluctuations is also a useful tool to study reionization. There exist fluctuations in the 21 cm brightness temperature due to fluctuations in the matter density, neutral fraction, and temperature. Fluctuations in the 21 cm brightness temperature are expected to be large near the edges of HI regions, and therefore may be more easily separated from the large Galactic foreground compared to the global signal, particularly near the end of reionization. The fluctuation in the brightness temperature  $\delta_{21} = \delta T_{\text{b}}/T_{\text{b}}$  is caused by fluctuations in the density field  $\delta$ , the neutral fraction  $\delta_{\text{HI}}$ , the Lyman- $\alpha$  flux  $\delta_{\alpha}$ , the radial velocity gradient  $\delta_{d_r v_r}$ , and the temperature  $\delta_{\text{T}}$ .<sup>105)</sup>

$$\begin{aligned} \delta_{21} = & \left[ 1 + \frac{x_c}{x_{\text{tot}}(1 + x_{\text{tot}})} \right] \delta + \frac{x_{\alpha}}{x_{\text{tot}}(1 + x_{\text{tot}})} \delta_{\alpha} + \delta_{\text{HI}} \\ & - \delta_{d_r v_r} + \delta_{\text{T}} \left( \frac{T_{\text{k}}}{T_{\text{k}} - T_{\gamma}} + \frac{x_{\alpha}}{x_{\text{tot}}(1 + x_{\text{tot}})} \frac{d \log \kappa_{10}}{d \log T_{\text{k}}} \right), \end{aligned} \quad (6.6)$$

where  $x_{\text{tot}} = x_c + x_{\alpha}$ , and  $\kappa_{10}(T_{\text{k}})$  is the collisional spin de-excitation rate coefficient.



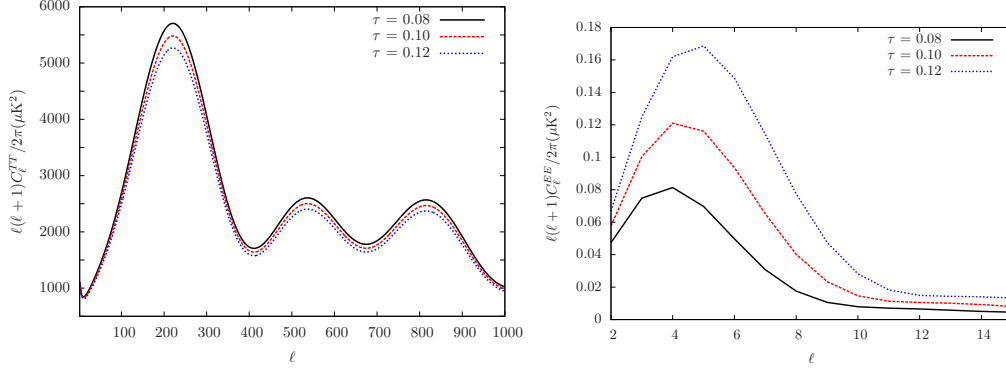


Fig. 9. CMB power spectra -  $TT$  and  $EE$  for different values of  $\tau$ . Scattering of CMB photons with free electrons results in a damping in the  $TT$  power spectrum, and a boost in the large angle  $EE$  power spectrum proportional to  $\tau^2$ .

The fluctuations in Fourier space may be expressed in the form:<sup>105)</sup>

$$\tilde{\delta}_{T_b}(\vec{k}) = \mu^2 \tilde{\delta}(\vec{k}) + \beta \tilde{\delta}(\vec{k}) + \tilde{\delta}_{\text{rad}}(\vec{k}), \quad (6.7)$$

where  $\mu$  is the cosine of the angle between the wave vector  $\vec{k}$  and the line of sight, while  $\beta$  is obtained by collecting together the terms in Eq. 6.6. Early results on reionization have been obtained by the PAPER experiment<sup>92)</sup> using the power spectrum of 21 cm observations. The PAPER experiment consists of 32 antennas, and collects data in South Africa. With an exposure of 55 days, PAPER obtained an upper limit on the 21 cm power spectrum of  $(52 \text{ mK})^2$  for  $k = 0.11 \text{ h/Mpc}$  at  $z=7.7$  at the  $2\sigma$  level.

## §7. Probing reionization with the cosmic microwave background

So far, we have discussed how the highly redshifted 21 cm radiation from neutral Hydrogen can probe early reionization. The cosmic microwave background is also an excellent probe of reionization. This is because free electrons scatter microwave photons, modifying the spectrum of anisotropies, and generating new, secondary anisotropies.

Scattering of CMB photons by free electrons leads to a damping in the temperature power spectrum by a factor  $\exp[-2\tau]$ . Unfortunately, this damping is largely degenerate with the amplitude of the primordial curvature power spectrum ( $A_s$  or  $\Delta_R^2$ ). This degeneracy is broken by polarization. Thomson scattering polarizes the CMB, and hence leads to a *boost* in the large angle  $EE$  power spectrum. Figure 9 shows the  $TT$  and  $EE$  power spectra for three different values of  $\tau$ . The Planck experiment (with WMAP polarization data included) has obtained a value of optical depth  $\tau = 0.089^{+0.012}_{-0.014}$ . The mean redshift of reionization is then  $z_* = 11.1 \pm 1.1$ . The *duration* of reionization is however, not well constrained by the polarization power spectrum.

Secondary scattering of CMB photons introduces additional power on small scales. High energy photons emitted from luminous sources ionize the region around

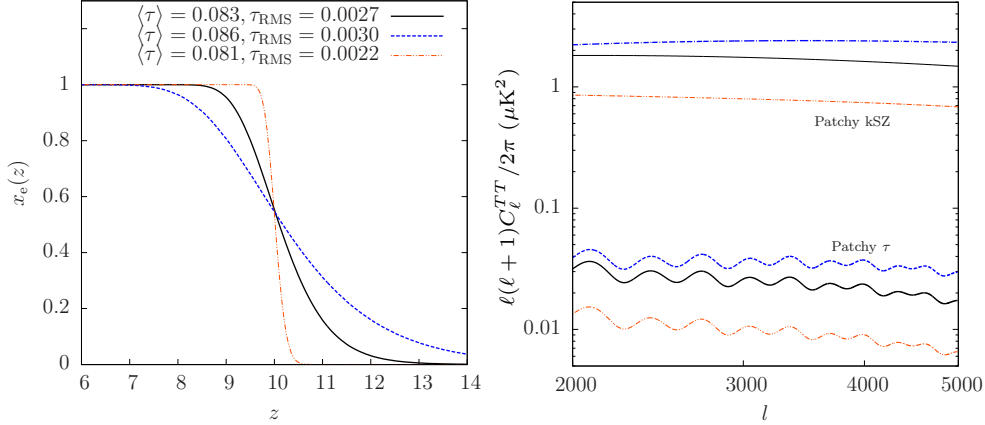


Fig. 10. Shown are three different reionization scenarios that have the same mean redshift of reionization, but different values of  $\langle \tau \rangle$  and  $\tau_{\text{RMS}}$ . The plot on the right shows the corresponding kSZ power spectra, and patchy  $\tau$  power spectra. From Ref. 112)

the sources, forming bubbles of hot ionized gas. Reionization is then said to be patchy, and the optical depth becomes a function of direction, i.e.  $\tau = \tau(\hat{n})$ , and can be described to lowest order by 2 quantities: the mean over angles  $\langle \tau \rangle$ , and the variance over angles, or equivalently, the root mean square value  $\tau_{\text{RMS}}$ . In the presence of a patchily reionized Universe, one observes a different CMB temperature when the line of sight passes through an ionized region, compared to a neutral region. An anisotropic optical depth therefore introduces “patchy screening” of the CMB, and hence secondary CMB power on small scales.

CMB photons scattering off moving electrons also introduces power on small scales, the well known Sunyaev-Zeldovich effect.<sup>106),107)</sup> When the electron velocity is due to thermal motion of gas atoms, it is known as the thermal Sunyaev-Zeldovich (tSZ) effect. The main contribution to the tSZ power comes from galaxy clusters. Scattering of CMB photons by free electrons with a bulk velocity (i.e. velocity relative to the Hubble flow) results in the kinetic Sunyaev-Zeldovich (kSZ) power. The fractional temperature change induced by electrons with a bulk motion along the line of sight is:<sup>108),109)</sup>

$$\frac{\Delta T}{T} = - \int c dt \left( \hat{n} \cdot \frac{\vec{v}}{c} \right) n_e \sigma_T e^{-\tau}, \quad (7.1)$$

where  $\hat{n}$  is a unit vector denoting the line of sight,  $\vec{v}$  is the peculiar velocity of the electrons,  $n_e$  is the number density of free electrons,  $\sigma_T$  is the Thomson cross section, and  $\tau$  is the optical depth. The homogeneous, linear contribution to the kSZ is called the Ostriker-Vishniac effect.<sup>108),109)</sup> In this approximation, the peculiar velocity  $\vec{v}$  may be simply expressed in terms of the matter overdensity. The Ostriker-Vishniac power spectrum may then be analytically computed (see for e.g.,<sup>110)</sup> and<sup>111)</sup>). The total kSZ is almost always larger than the Ostriker-Vishniac power due to nonlinearities, and patchiness in the reionization field. The patchy component of the kSZ due to a patchily reionized Universe is a good probe of the *duration* of reionization.



Figure 10 (left) shows three different non-instantaneous reionization scenarios, assuming single step reionization (from Ref.<sup>112</sup>). These three reionization histories have the same mean reionization redshift, but different mean values  $\langle\tau\rangle$ , as well as different durations, and hence different values of  $\tau_{\text{RMS}}$ . The short reionization scenario has  $\langle\tau\rangle = 0.081$ ,  $\tau_{\text{RMS}} = 0.0022$ , the fiducial model has  $\langle\tau\rangle = 0.083$ ,  $\tau_{\text{RMS}} = 0.0027$ , and the extended reionization model has  $\langle\tau\rangle = 0.086$ ,  $\tau_{\text{RMS}} = 0.0030$ . These values of  $\tau_{\text{RMS}}$  are representative of what is seen in realistic numerical simulations. The plot on the right shows the corresponding values of patchy kSZ as well as excess power due to patchy  $\tau$ , for the three reionization models. Using large scale numerical simulations, authors<sup>113),114)</sup> found an approximate scaling relation for the patchy kSZ power:

$$D_{\ell=3000}^{kSZ} \approx 2.02 \mu\text{K}^2 \left[ \left( \frac{1+\bar{z}}{11} \right) - 0.12 \right] \left( \frac{\Delta_z}{1.05} \right)^{0.47}, \quad (7.2)$$

where  $D_\ell = l(l+1)C_l/2\pi$ , and  $\Delta z = [z(x_e = 25\%) - z(x_e = 75\%)]$ .

### 7.1. Detecting patchy reionization through cross correlation of the CMB

Let us now consider a different technique to probe patchy reionization. Since the damping term  $\exp[-\tau(\hat{n})]$  multiplies the primary CMB temperature  $T$ , the effect of patchy reionization is largest when  $|T|$  is large, i.e. on degree scales. *Patchy reionization therefore transfers CMB power from large scales to small scales.* This results in a non-zero correlation between large and small scales. This “patchy  $\tau$  correlator” is far more sensitive to patchy reionization than the power spectrum.

To compute the patchy  $\tau$  correlator, we begin by filtering the CMB into 2 maps: (i) A map with information only on large scales, i.e. multipoles  $\ell < \ell_{\text{boundary1}}$ , and (ii) A map with information only on small scales,  $\ell > \ell_{\text{boundary2}}$ . The 2 maps are then squared:  $f = T^2(\ell < \ell_{\text{boundary1}})$ ,  $g = T^2(\ell > \ell_{\text{boundary2}})$ . The patchy  $\tau$  correlator is then simply  $\langle\delta f \delta g\rangle$ , where  $\delta f = f - \langle f\rangle$ , and  $\delta g = g - \langle g\rangle$  are fluctuations in the squared CMB temperature obtained from the filtered maps. The angle brackets denote an average over the map. Let us first examine a simple model wherein we ignore all secondaries besides patchy reionization. Let  $\theta_{\text{obs}}(\hat{n})$  be the observed CMB temperature fluctuation, and let  $\theta_{\text{cmb}}(\hat{n})$  be the primordial CMB fluctuation.  $\theta_{\text{cmb}}$  consists of large scale and small scale modes, i.e.  $\theta_{\text{cmb}} = \theta_L + \theta_S$ . The optical depth is  $\tau(\hat{n}) = \langle\tau\rangle + \delta\tau(\hat{n})$ .

The observed fluctuation is then given by  $\theta_{\text{obs}}(\hat{n}) = \theta_{\text{cmb}}(\hat{n}) \times \exp[-\delta\tau(\hat{n})] \approx \theta_{\text{cmb}}(\hat{n}) - \delta\tau(\hat{n})\theta_{\text{cmb}}(\hat{n})$ , where we have dropped the constant term  $\exp[-\langle\tau\rangle]$  because it is an overall multiplicative constant. The  $\delta\tau(\hat{n})$  fluctuations are on scales much smaller than the primary CMB fluctuations. When the observed CMB map is filtered, we obtain a large scale map  $\theta_L$ , and a small scale map  $\theta_S + \theta_L\delta\tau$ . The large scale and small scale modes of the CMB are independent of each other, and are therefore uncorrelated. The  $\delta\tau(\hat{n})$  field is also uncorrelated with the CMB fluctuations. The patchy  $\tau$  correlator is therefore simply  $\langle\delta f \delta g\rangle = \langle\delta\tau^2\rangle \times (\langle\theta_L^4\rangle - \langle\theta_L^2\rangle^2)$ . The patchy  $\tau$  correlator is thus sensitive to optical depth fluctuations and vanishes in the limit of homogeneous reionization.

Figure 11 (from Ref. 112)) shows the patchy  $\tau$  correlator in units of  $\mu K^4$ , with

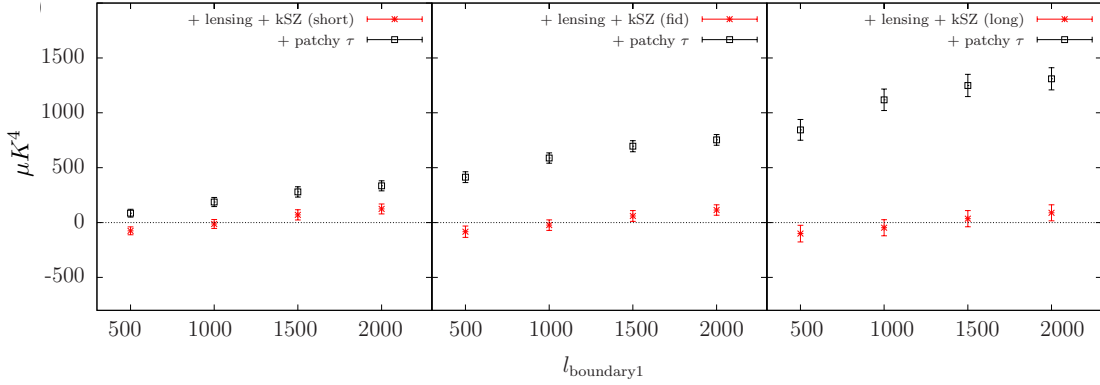


Fig. 11. The patchy  $\tau$  correlator for different reionization scenarios. The CMB maps were obtained using HEALPIX,<sup>118)</sup> and the patchy  $\tau$  maps were obtained from numerical simulations.<sup>113)</sup> Only kSZ and lensing have been included. It is easy to distinguish even small values of patchy  $\tau$  when the larger secondary components have been removed through a multi-frequency analysis. From Ref. 112).

and without patchy reionization. The CMB maps were simulated using the HEALPIX software.<sup>118)</sup> The patchy reionization map was obtained using numerical simulations. The boundary for the large scale map  $l_{\text{boundary1}}$  is varied from 500 - 2000. The small scale map includes multipoles from 3000-5000. The maps shown in Figure 11 include kSZ and lensing, but do not include tSZ, CIB, or radio contributions. Thus, we assume that the large frequency dependent contaminations may be removed through a multi-frequency analysis of the data. The three panels are plotted for the 3 reionization scenarios shown in Figure 10.

Since different multipoles of the primary CMB provide independent information, the correlation between large and small scale maps is zero for the primary CMB. Including the effect of CMB lensing however results in a non-zero cross correlation, because lensing of the CMB results in a redistribution of power, transferring CMB power from large scales to small scales. The cross correlation due to lensing is negative for small  $l_{\text{boundary1}}$ , and increases, passing through zero at  $l_{\text{boundary1}} \sim 1200$ . The patchy  $\tau$  term is similarly correlated. The cross correlation due to patchy  $\tau$  is always positive and increases with  $l_{\text{boundary1}}$ . Moreover the patchy  $\tau$  terms contributes significantly more to the cross correlation than the lensing term. Thus, one can detect patchy reionization at high significance by computing the cross correlation between the squared maps. It is however, much harder to measure the patchy  $\tau$  correlator when other secondaries such as tSZ, CIB, and radio contributions are present.<sup>112)</sup>

## §8. Future prospects

A number of observational programs are aimed at detecting the signatures of reionization in the CMB. Data from the Planck mission will deliver accurate measurement of the CMB polarization and the total Thomson optical depth, from which

details of reionization can be derived.<sup>53),54)</sup> Ongoing experiments such as ACTPol<sup>116)</sup> and SPTPol<sup>117)</sup> will be able to measure the kinematic Sunyaev-Zeldovich effect to higher accuracy. The Cosmology Large Angular Scale Surveyor (CLASS)<sup>123)</sup> and the Primordial Inflation Polarization Explorer (PIPER)<sup>124)</sup> are designed to measure the primordial  $B$  mode polarization of the CMB, but they will also have the sensitivity to measure the  $E$  mode to very high accuracy. The CLASS instrument has a field of view of  $19^\circ \times 14^\circ$  with a resolution of  $1.5^\circ$  FWHM, and will measure the polarization of the CMB at 40, 90, and 150 GHz from Cerro Toco in the Atacama desert of northern Chile. PIPER is a balloon based experiment, and will fly in both the northern and southern hemispheres, achieving a sky coverage of 85%. With 5120 detectors, PIPER is expected to obtain noise residuals less than 2.7 nK with 100 hours of observation. These experiments will significantly improve our understanding of the reionization history of the Universe through precise measurements of the large angle polarization of the CMB.

Future observations of the CMB spectral distortion will open a new window to probe the characteristic spectral energy distribution of the dominant sources of reionization, e.g. by the Primordial Inflation Explorer (PIXIE),<sup>125)</sup> and the Polarized Radiation Imaging and Spectroscopy Mission (PRISM).<sup>119)</sup> Heating of gas by early stars results in a Compton- $y$  distortion proportional to the temperature of the gas and the reionization optical depth. PIXIE is expected to measure the Compton distortion to an accuracy  $y < 2 \times 10^{-9}$ . In combination with PIXIE's measurement of the optical depth, PIXIE can determine the temperature of the intergalactic medium to 5% precision at  $z=11$ .<sup>125)</sup> In fact any form of energy injection to the CMB can be studied to unprecedented accuracy, and hence decay or annihilation of dark matter particles, for example, can be inferred from the exact shape of the distortion that encodes the time when dark matter decay/annihilation occurred.<sup>122)</sup>

The abundances of light element atoms and ions such as OI, NII, CII can be measured, in principle, by utilizing the characteristic CMB spectral (frequency-dependent) signatures and angular fluctuations generated by the resonant scattering and fine structure line emission.<sup>120),121)</sup> Assuming that the first sources of light are also the first sources of the metals, one can trace the early star-formation history from CMB observations.

Altogether, we have very good prospects that there will be significant progress in the study of the Dark Ages in the next two decades, when next-generation radio telescope arrays and space-borne CMB experiments probe the distribution of the intergalactic gas in the early universe.

### Acknowledgements

The present work is supported in part by the Grants-in-Aid by the Ministry of Education, Science and Culture of Japan (25287050: NY). A.N. was funded by NASA grant NNX14AB57G. A.N. acknowledges partial financial support from the Pittsburgh Particle physics, Astrophysics, and Cosmology Center, and the Department of Physics and Astronomy at the University of Pittsburgh. Portions of this research were conducted at the Jet Propulsion Laboratory, California Institute of

Technology, which is supported by the National Aeronautics and Space Administration (NASA).

### References

- 1) J. E. Gunn, B. A. Peterson, *ApJ* **142**, 1633 (1965)
- 2) X. Fan et al. *Astron. J.*, **122**, 2833 (2001)
- 3) G. Hinshaw et al., *ApJS* **208**, 19 (2013)
- 4) X. Fan, *Research in Astronomy and Astrophysics* **12** 865 (2012).
- 5) M. F. Morales, J. S. B. Wythe, *ARAA* **48** 127 (2010).
- 6) D. H. D. Lyth & A. A. Riotto, *Physics Reports* **314**, 1 (1999).
- 7) N. Yoshida, T. Hosokawa, K. Omukai, *PTEP*, **2012a** 305 (2012)
- 8) J. Miralda-Escude, *Science* **300**, 1904 (2003).
- 9) L. Gao, N. Yoshida, T. Abel, C. S. Frenk, A. Jenkins, & V. Springel, *M.N.R.A.S.* **378**, 449 (2007)
- 10) S. Hirano et al. *Astrophys. J.*, **395**, 777 (2014)
- 11) M. Tokutani, N. Yoshida, S.-P. Oh, N. Sugiyama, *Astrophys. J.*, **395**, 777 (2009)
- 12) H. Park et al. *ApJ*, **769**, 93 (2013)
- 13) S. Zaroubi et al. *MNRAS*, **425**, 2964 (2012)
- 14) T. Greif et al. *MNRAS*, **399**, 639 (2009)
- 15) M. Ricotti, J. P. Ostriker, *MNRAS*, **352**, 547 (2004)
- 16) M. Kuhlen, P. Madau, R. Montgomery, *ApJ*, **637**, 1 (2006)
- 17) J. Miralda-Escude, M. Haehnelt, M. J. Rees, *ApJ*, **530**, 1 (2000)
- 18) M. Valdes, C. Evoli, A. Messinger, A. Ferrara, N. Yoshida, *MNRAS*, **429**, 1705 (2012)
- 19) D. Finkbeiner, S. Galli, T. Lin, T. R. Slatyer, *PRD*, **85**, 3522 (2012)
- 20) C. Shultz, J. Onorbe, K. N. Abazajian, J. S. Bullock, arXiv:1401.3769
- 21) N. Yoshida, A. Sokasian, L. Hernquist, and V. Springel, *Astrophys. J.* **591**, L1 (2003)
- 22) V. Bromm, N. Yoshida, *ARAA* **49**, 373 (2011).
- 23) N. Yoshida, T. Abel, L. Hernquist, and N. Sugiyama, *Astrophys. J.* **592**, 645 (2003)
- 24) P. R. Shapiro, K. Ahn, M. A. Alvarez, I. T. Iliev, H. Martel, & D. Ryu, *Astrophys. J.* **646**, 681 (2006)
- 25) R. J. Bouwens et al. *Astrophys. J.* **765**, 16 (2013)
- 26) R. S. Ellis et al. *Astrophys. J.* **763**, 7 (2013)
- 27) B. E. Robertson, R. S. Ellis, J. S. Dunlop, R. J. McLure, D. P. Stark, *Nature* **468** (2010) 49
- 28) S. Finkelstein et al. *Astrophys. J.* **758**, 93 (2012)
- 29) S.-P. Oh, *Astrophys. J.* **569**, 558 (2001)
- 30) A. Natarajan, D.J. Schwarz, *Phys. Rev. D* **78**, 103524 (2008)
- 31) A. Natarajan, D.J. Schwarz, *Phys. Rev. D* **80**, 043529 (2009)
- 32) A. Natarajan, D.J. Schwarz, *Phys. Rev. D* **81**, 123510 (2010)
- 33) D. Spolyar, K. Freese, P. Gondolo, *Phys. Rev. Lett.* **100**, 051101 (2008)
- 34) F. Iocco, *Astrophys. J.* **677**, L1 (2008)
- 35) A. Natarajan, J.C. Tan, B.W. O'Shea, Brian W., *Astrophys. J.* **692**, 574 (2009)
- 36) S. Hirano, H. Umeda, N. Yoshida, *Astrophys. J.* **736**, 10 (2011)
- 37) S. Galli, F. Iocco, G. Bertone, A. Melchiorri, *Phys. Rev. D* **80**, 023505 (2009)
- 38) A. Natarajan, *Phys. Rev. D*, **85**, 083517 (2012)
- 39) K. Ahn, *M.N.R.A.S.* **375**, 881 (2007)
- 40) T. Matsumoto et al. *Astrophys. J.* **626** 31 (2005)
- 41) F. Aharonian et al. *Nature* **440** 1018 (2006)
- 42) A. Kashlinsky et al. *Astrophys. J.* **753** 63 (2012)
- 43) T. Matsumoto et al. *Astrophys. J.* **742** 124 (2011)
- 44) E. R. Fernandez et al. *Astrophys. J.* **750** 20 (2012)
- 45) H. Dole et al. *Astron. Astrophys.* **451** 417 (2006)
- 46) E. R. Fernandez, S. Zaroubi *MNRAS* **433** 2047 (2013)
- 47) A. Cooray et al. *Nature* **490** 514 (2012)
- 48) N. Cappelluti et al. *ApJ* **769** 68 (2013)
- 49) T. Kitayama, N. Yoshida, H. Susa, and M. Umemura, *Astrophys. J.* **613**, 631 (2004)
- 50) D. Whalen, T. Abel, and M. L. Norman, *Astrophys. J.* **610**, 14 (2004)

- 51) E. Komatsu et al., *Astrophys. J.* **192** (2011) 18
- 52) L. Hui & Z. Haiman, *Astrophys. J.* **596**, 9 (2003)
- 53) G. P. Holder et al. *Astrophys. J.* **595**, 13 (2003)
- 54) P. Mukherjee, A. R. Liddle, *MNRAS* **389**, 231 (2008)
- 55) X. Fan et al. *Astron. J.*, **123**, 1247 (2002)
- 56) R. H. Becker et al. *Astron. J.*, **122**, 2850 (2001)
- 57) L. Pentericci et al. *Astron. J.*, **123**, 2151 (2002)
- 58) D. Larson et al. *Astrophys. J.S.*, **192**, 16 (2011)
- 59) J. Tumlinson, J. M. Shull, *Astrophys. J.* **528**, L65 (2000)
- 60) A. Loeb, R. Barkana, *Ann. Rev. Astron. Astrophys.*, **39**, 19 (2001)
- 61) R. Barkana, A. Loeb, *Phys. Rep.*, **349**, 125 (2001)
- 62) J. S. B. Wyithe, A. Loeb, *Astrophys. J.*, **588**, L69 (2003)
- 63) Ciardi, B., Ferrara, A., S. D. M. White, *M.N.R.A.S.*, **344**, L7 (2003)
- 64) A. Sokasian, N. Yoshida, T. Abel, L. Hernquist, V. Springel, *M.N.R.A.S.*, **350**, 47 (2004)
- 65) A. Loeb,, M. Zardarriaga, *Phys. Rev. Lett.*, **92**, 211301 (2004)
- 66) A. Cooray, *Phys. Rev. D*, **70**, 063509 (2004)
- 67) S. Bharadwaj, S. S. Ali, *M.N.R.A.S.*, **352**, 142 (2004)
- 68) C. L. Carilli, S. R. Furlanetto, F. Briggs, M. Jarvis, S. Rawlings, H. Falcke, *New Astron. Rev.* **48**, 1029 (2004)
- 69) S. R. Furlanetto, S.-P. Oh, F. Briggs *Physics Reports* **433** (2006) 181
- 70) S. R. Furlanetto, F. H. Briggs, *New Astron. Rev.* **48**, 1039 (2004)
- 71) J. R. Pritchard, A. Loeb, *Phys. Rev. D*, **82**, 023006 (2010)
- 72) J. R. Pritchard, A. Loeb, *Reports on Progress in Physics*, **75**, 086901 (2012)
- 73) A. Liu, J. R. Pritchard, M. Tegmark, A. Loeb, *Phys. Rev. D* **87**, 043002 (2013)
- 74) S. A. Wouthuysen *Astronomical Journal*, **57**, 31 (1952)
- 75) G. B. Field *Proceedings of the IRE*, **46**, 240 (1958)
- 76) P. A. Shaver, R. A. Windhorst, P. Madau, A.G. de Bruyn, *Astron. Astrophys.* **345**, 380 (1999)
- 77) P. Madau, A. Meiksin, M.J. Rees, *Astrophys. J.* **475**, 429 (1997)
- 78) P. Tozzi, P. Madau, A. Meiksin, M. J. Rees *Astrophys. J.*, **528**, 597 (2000)
- 79) A. Liu, J. R. Pritchard, M. Tegmark, A. Loeb, *Phys. Rev. D.* **87**, 043002 (2013)
- 80) R. Barkana, A. Loeb,, *Astrophys. J.* **626**, 1 (2005)
- 81) A. L. Muratov, O. Y. Gnedin, N. Y. Gnedin, M. Zemp, *Astrophys. J.*, **773**, 19 (2013)
- 82) V. Bromm, R. P. Kudritzki, A. Loeb, *Astrophys. J.*, **552**, 464 (2001)
- 83) S. R. Furlanetto, S.-P. Oh, F. H. Briggs, *Phys. Rep.* **433**, 181 (2006)
- 84) A. Mesinger, S. R. Furlanetto, R. Cen, *M.N.R.A.S.*, **411**, 955 (2011)
- 85) M. G. Santos, A. Amblard, J. Pritchard, H. Trac, R. Cen, A. Cooray, *Astrophys. J.*, **689**, 1 (2008)
- 86) M.G. Santos, L. Ferramacho, M.B. Silva, A. Amblard, A. Cooray, *M.N.R.A.S.*, **406**, 2421 (2010)
- 87) S. Furlanetto, R., Stoeve, S.J. *Mon. Not. R. Astron. Soc.* **404**, 1869 (2010)
- 88) J.M. Shull, M.E. Van Steenberg *Astrophys. J.* **298**, 268 (1985)
- 89) T. Kanzaki, M. Kawasaki *Phys. Rev. D* **78**, 103004 (2008)
- 90) M. Valdés, C. Evoli, A. Ferrara *Mon. Not. R. Astron. Soc.* **404**, 1569 (2010)
- 91) J.C. Pober, et al., *Astrophys. J.*, **768**, L36 (2013)
- 92) A. R. Parsons, et al. arXiv:1304.4991 (2013)
- 93) G. Paciga et al., *M.N.R.A.S.*, **413**, 1174 (2011)
- 94) M. P. van Haarlem et al., *Astron. Astrophys.*, **556**, A2 (2013)
- 95) G. Bernardi, et al., *ApJ*, **771**, 105 (2013)
- 96) Hydrogen Epoch of Reionization Array (HERA), [http://reionization.org/RFI2 HERA.pdf](http://reionization.org/RFI2%20HERA.pdf)
- 97) Square Kilometer Array (SKA) <http://www.skatelescope.org/>
- 98) J. D. Bowman, A. E. E. Rogers, J. N. Hewitt, *Astrophys. J.*, **676**, 1 (2008)
- 99) Large Aperture Experiment to detect the Dark Ages (LEDA) <http://www.cfa.harvard.edu/LEDA/science.html>
- 100) T.C. Voytek, A. Natarajan, J.M.J. García, J.B. Peterson O. López-Cruz *Astrophys. J. Lett.*, **782**, L9 (2014)
- 101) J.O. Burns, J. Lazio, S. Bale, J. Bowman, R. Bradley, C. Carilli, S. Furlanetto, G. Harker, A. Loeb, J. Pritchard *Advances in Space Research*, **49**, 433 (2012)
- 102) A. de Oliveira-Costa, M. Tegmark, B.M. Gaensler, J. Jonas Landecker, T. L., Reich, P.

- M.N.R.A.S.* **388**, 247 (2008)
- 103) L.J. Greenhill, G. Bernardi, arXiv:1201.1700 (2012)
  - 104) M.A. Clark, P.C. La Plante, L.J. Greenhill, arXiv:1107.4264 (2011)
  - 105) R. Barkana, A. Loeb,, *Astrophys. J.* **624**, L65 (2005)
  - 106) R.A. Sunyaev, Y.B. Zeldovich, *Mon. Not. R. Astron. Soc.*, **190**, 413 (1980)
  - 107) Y.B. Zeldovich, R.A. Sunyaev, *Astrophysics and Space Science*, **4**, 301 (1969)
  - 108) J.P. Ostriker, E.T. Vishniac, *Astrophys. J.*, **306**, L51 (1986)
  - 109) E.T. Vishniac, *Astrophys. J.*, **322**, 597 (1987)
  - 110) A.H. Jaffe, M. Kamionkowski, *Phys. Rev. D*, **58**, 043001 (1998)
  - 111) K.G. Lee, *arXiv:0902.1530* (2009)
  - 112) A. Natarajan, N. Battaglia, H. Trac, U.-L. Pen, A. Loeb, *Astrophys. J.* **776**, 82 (2013)
  - 113) N. Battaglia, H. Trac, R. Cen, A. Loeb, *Astrophys. J.*, **776**, 81 (2013)
  - 114) N. Battaglia, A. Natarajan, H. Trac, R. Cen, A. Loeb, *Astrophys. J.*, **776**, 83 (2013)
  - 115) O. Zahn, et al. *Astrophys. J.*, **756**, 65 (2012)
  - 116) M.D. Niemack, et al. *Society of Photo-Optical Instrumentation Engineers (SPIE) Conference Series*, **7741** (2010)
  - 117) J.E. Austerlmann, et al. *Society of Photo-Optical Instrumentation Engineers (SPIE) Conference Series*, **8452** (2012)
  - 118) K.M. Górski, E. Hivon, A. J. Banday, B.D. Wandelt, F.K. Hansen, M. Reinecke, M. Bartelmann, *Astrophys. J.* **622**, 759 (2005)
  - 119) P. Andre et al. *JCAP* **02**, 006 (2014).
  - 120) K. Basu, C. Hernandez-Monteagudo, R. A. Sunyaev, *Astron. Astrophys.* **416**, 447 (2004).
  - 121) C. Hernandez-Monteagudo, R. A. Sunyaev, *MNRAS* **359** 597 (2005)
  - 122) R. Khatri, R. A. Sunyaev, *JCAP* **09**, 016 (2012)
  - 123) J.R.Eimer, C.L. Bennett, D.T. Chuss, T. Marriage, E.J. Wollack, L. Zeng, Society of Photo-Optical Instrumentation Engineers (SPIE) Conference Series, **8452** (2012)
  - 124) A. Kogut, et al., Society of Photo-Optical Instrumentation Engineers (SPIE) Conference Series, **8452** (2012)
  - 125) A. Kogut, D.J. Fixsen, D.T. Chuss, J. Dotson, E. Dwek, M. Halpern, G.F. Hinshaw, S.M. Meyer, S.H. Moseley, M.D. Seiffert, D.N. Spergel, E.J. Wollack, *JCAP* **025** (2011)